CHEMISTRY
A EUROPEAN JOURNAL

ChemPubSoc
Europe

DOI: 10.1002/chem.201200254

# Nonlinear Absorbing Platinum(II) Diimine Complexes: Synthesis, Photophysics, and Reverse Saturable Absorption

**Rui Liu,[a] Dapeng Zhou,[b] Alexander Azenkeng,[c] Zhongjing Li,[a] Yuhao Li,[a] Ksenija D. Glusac,[b] and Wenfang Sun*[a]**

**Abstract:** A series of platinum(II) diimine complexes with different substituents on fluorenyl acetylide ligands (**1a**–**1e**) were synthesized and characterized. The influence of the auxiliary substituent on the photophysics of these complexes has been systematically investigated spectroscopically and theoretically (using density functional theory (DFT) methods). All complexes exhibit ligand-centered $^1\pi,\pi^*$ transitions in the UV and blue spectral region, and broad, structureless $^1$MLCT/$^1$LLCT (**1a**, **1b**, **1d** and **1e**) or $^1$MLCT/$^1$LLCT/$^1\pi,\pi^*$ (**1c**) absorption bands in the visible region. All complexes are emissive in solution at room temperature, with the emitting state is tentatively assigned to mixed $^3$MLCT/$^3\pi,\pi^*$ states. The degree of $^3\pi,\pi^*$ and $^3$MLCT mixing varies with different substituents and solvent polarities. Complexes **1a**–**1e** exhibit relatively strong singlet and triplet transient absorption from 450 to 800 nm, at which point reverse saturable absorption (RSA) could occur. Nonlinear transmission experiments at 532 nm by using nanosecond laser pulses demonstrate that **1a**–**1e** are strong reverse saturable absorbers and could potentially be used as broadband nonlinear absorbing materials.

**Keywords:** fluorenylacetylide ligands · nonlinear absorbing materials · photophysics · platinum · synthesis

## Introduction

Platinum(II) diimine acetylide complexes have attracted a great deal of attention due to their potential applications in photoinduced charge separation,[1] chemosensors,[2] and luminescent materials.[3] These applications are intrinsically based on the square-planar configuration of the complexes, the presence of multiple intramolecular charge-transfer states, the low-energy metal-to-ligand or ligand-to-ligand charge-transfer absorption, and the long-lived triplet emission. Furthermore, the structures of these complexes can be readily modified; this provides an additional opportunity to tune the properties of the platinum complexes by varying the substituents on either the bipyridine or acetylide ligands.[4] Previous studies on $Pt^{II}$ diimine acetylide complexes have shown that the energy of the metal-to-ligand charge-transfer ($^1$MLCT) band decreases when the electron-withdrawing ability of the substituent on the bipyridine ligand increases or when the electron-donating ability of the substituents on the acetylide ligands increases. However, no clear trend in the emission energy, lifetime and quantum yield was found when the substituents on the acetylide ligands were changed, due to the admixture of the $^3$MLCT and $^3\pi,\pi$ states. By modifying the acetylide ligands, the emissive excited state could originate from a $^3$MLCT state,[3a] a $^3\pi,\pi$ state localized on two acetylide ligands,[4c] a $^3\pi,\pi$ state localized on one of the acetylide ligands,[5] or a mixture of the $^3$MLCT and $^3\pi,\pi$ state.[3c] Moreover, the order of the $^3$MLCT and $^3\pi,\pi$ state could be switched in solvent with different polarities.[3b]

Although many of these previous studies are intriguing, reports on nonlinear optical application of $Pt^{II}$ diimine complexes, especially as nonlinear transmission materials based on reverse saturable absorption, are still quite limited. Platinum diimine complexes reported by Schanze's[4c,5] and Castellano's groups[2b,3b,c] possess broadband triplet excited-state absorption, and are expected to exhibit reverse saturable absorption in the visible spectral region. To demonstrate the feasibility of using $Pt^{II}$ diimine acetylide complexes as reverse saturable absorbers for nonlinear transmission applications, our group recently reported the synthesis and nonlinear absorption of a platinum 2,2′-bipyridine complex bearing 2-(benzothiazol-2′-yl)-9,9-diethyl-7-ethynylfluorene ligands.[6] This complex exhibited remarkable reverse saturable absorption and the largest ratios of the excited-state absorption cross-section to the ground-state absorption cross-section in the visible spectral region among all of the reported reverse saturable absorbers and the largest two-photon absorption cross-sections in the near-IR region for platinum

[a] Dr. R. Liu, Z. Li, Dr. Y. Li, Prof. W. Sun
Department of Chemistry and Biochemistry
North Dakota State University, Fargo, ND 58108-6050 (USA)
Fax: (+1) 701-231-8831
E-mail: Wenfang.Sun@ndsu.edu

[b] D. Zhou, Prof. K. D. Glusac
Department of Chemistry, Bowling Green State University
Bowling Green, OH 43403-0001 (USA)

[c] Dr. A. Azenkeng
Energy and Environmental Research Center
University of North Dakota, Grand Forks, ND 58202-9018 (USA)

Supporting information for this article is available on the WWW under http://dx.doi.org/10.1002/chem.201200254.

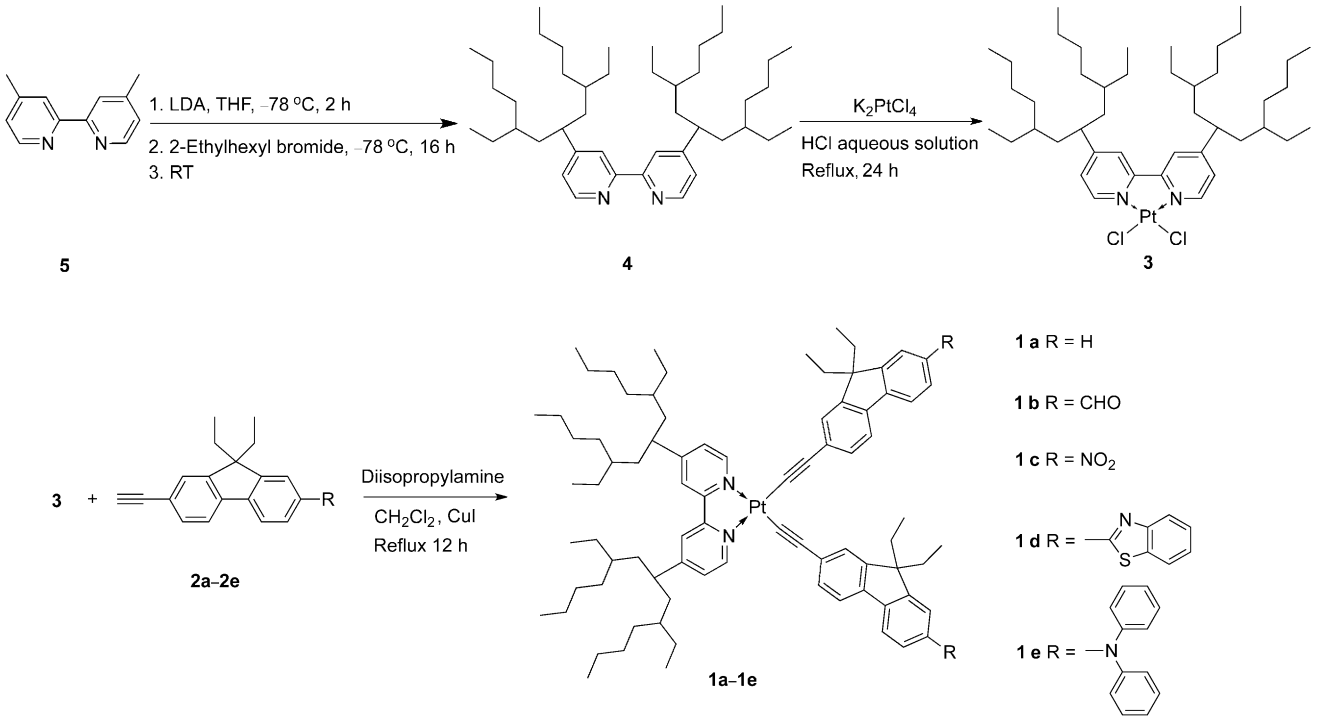


Scheme 1. Synthesis route for complexes **1a**–**1e**.

complexes reported to date.[6] Although this result is quite exciting, we seek to improve the nonlinear absorption by structural modification. To reach this goal, understanding the structure–property correlation becomes critical.

In this work, we designed and synthesized a series of new platinum diimine complexes with different substituents on the fluorene component. The synthesis route and the structures of the target complexes are displayed in Scheme 1. The $NPh_2$ group was chosen as the electron-donating substituent and the $NO_2$, CHO, and benzothiazole (BTZ) groups were chosen as electron-withdrawing substituents. In addition, branched alkyl chains were introduced on bipyridine ligand to reduce the intermolecular aggregation and improve the solubility of the $Pt^{II}$ complexes. The photophysical properties of these complexes were systematically investigated with the aim of understanding the structure–property correlations and developing novel nonlinear absorbing materials with enhanced reverse saturable absorption and two-photon absorption.

## Results and Discussion

**Synthesis**: Scheme 1 outlines the synthesis route for complexes **1a**–**1e**. The 2-ethynyl-7-*R*-9,9-diethylfluorene ligands (**2a**–**2e**) were synthesized according to literature procedures.[8–10] The bipyridyl platinum chloride complex ($bpyPtCl_2$, **3**) was also synthesized by following literature procedure.[11] Sonogashira reaction conditions (terminal alkyne, CuI/$iPr_2NH$/$CH_2Cl_2$) were used to prepare **1a**–**1e** from the respective acetylene ligand and the $bpyPtCl_2$ precursor. A yield of 53–61 % was obtained after recrystallization for the last step reaction that converts **2** and **3** to the final product **1**. All complexes (**1a**–**1e**) are air-stable and soluble in $CH_2Cl_2$, $CHCl_3$, acetone, tetrahydrofuran, toluene, DMF and dimethyl sulfoxide. $^1$H NMR spectra and elemental analyses confirmed the proposed structures for complexes **1a**–**1e**. HRMS data were not obtained because of the difficulty to ionize the samples although different methods were attempted. The $^1$H NMR spectroscopy data for all of the complexes are consistent with the assigned structures and previously reported complexes of similar type.[2b,3b,4c,5,6a] The bipyridine resonances ($\delta = 7.8$–$9.9$ ppm) are particularly informative because they substantially downfield-shift upon coordination with the $Pt^{II}$ metal ion and upon exchange of chloride for acetylide as the co-ligands, especially the protons adjacent to the coordination sites.

**Electronic absorption**: The electronic absorptions of **1a**–**1e** and **2a**–**2e** obey Lambert–Beer's law in the concentration range used in our study ($1\times10^{-6}$–$1\times10^{-4}$ mol L$^{-1}$), indicating that no ground-state aggregation occurs in this concentration range. The UV/Vis absorption spectra of **1a**–**1e** in $CH_2Cl_2$ are illustrated in Figure 1, and their absorption band maxima and molar extinction coefficients are presented in Table 1. Similar to the platinum(II) diimine acetylide complexes reported previously, the intense absorption bands below 380 nm can be assigned to the $^1\pi,\pi^*$ transitions of the acetylide ligands.[2b,3b,5,6a] The similarity in the energy of these bands to those of their respective acetylide ligands and the minor solvent effect both support this assignment (Supporting Information Figures S1–S6). However, these

  

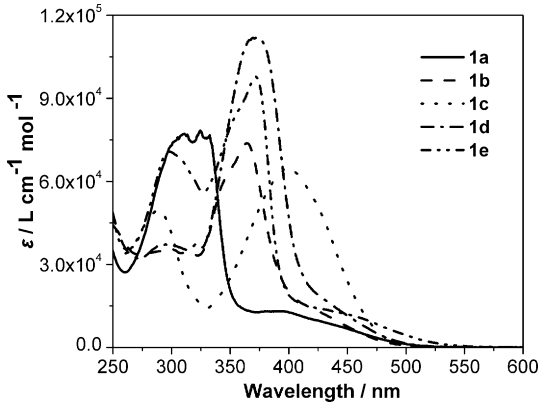


Figure 1. UV/Vis absorption spectra of **1a**–**1e** in $CH_2Cl_2$

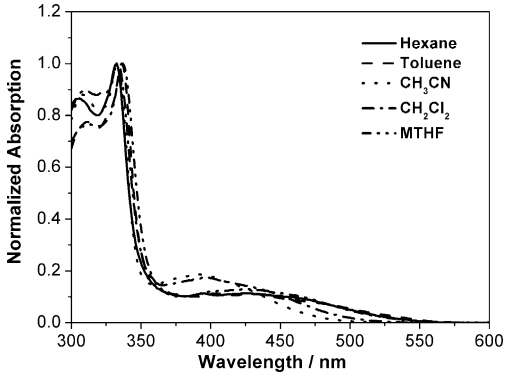


Figure 2. Normalized UV/Vis absorption spectra of **1a** in different solvents.

bands exhibit clear bathochromic shift compared to those of their ligands, implying some delocalization of the ligand-centered molecular orbitals via interactions with the platinum dπ orbitals. In addition, complex **1d** shows less vibronic structure in this band, which is indicative of weak electron-vibronic coupling and is also consistent with a delocalized excited state.[5,6a]

In addition, each complex possesses a broad, moderately intense absorption band at 400–550 nm, except for complex **1c**. These low-energy absorption bands shift to longer wavelengths in less polar solvents (i.e., hexane and toluene) compared to those in more polar solvents (i.e., $CH_3CN$ and $CH_2Cl_2$), as exemplified in Figure 2 for complex **1a**. This negative solvatochromic effect is indicative of a charge-transfer transition in which the dipole moment of the ground state is larger than that of the excited state. Based on similar results reported for other platinum diimine acetylide complexes and our density functional theory (DFT) calculation results, which will be discussed later, these bands can be attributed to the $^1$MLCT/$^1$LLCT transitions.[3,4c,5,6] The spectrum of **1c**, which is dominated by an intense, structureless absorption band at $\lambda_{max}=397$ nm ($\varepsilon \approx 6.5\times 10^4$ L mol$^{-1}$ cm$^{-1}$), is significantly different from those of the other complexes. Considering the large molar extinction coefficient and similar features to that of the $Pt^{II}$ diimine complex with nitrostilbenylacetylide ligands, this band could be attributed to $^1$MLCT/$^1$LLCT transitions mixed with a significant $^1\pi,\pi^*$ transition component.[7]

The lowest energy absorption band is influenced significantly by the auxiliary substituent on the acetylide ligands. Both electron-donating and electron-withdrawing substituents on the fluorene component cause a pronounced red-shift of this band compared to that of complex **1a**. Furthermore, the energy of the $^1$MLCT/$^1$LLCT band decreases when the electron-donating ability of the substituents on the acetylide ligands increases. As demonstrated by complex **1e**, electron-donating substituent $NPh_2$ causes a pronounced red-shift of this transition compared with the electron-withdrawing substituents, such as the CHO, $NO_2$, and BTZ groups. The assignment of this lowest energy absorption band is supported by DFT calculations discussed in the following section.

Table 1. Photophysical parameters of **1a**–**1e**.

| | $\lambda_{abs}$ [nm] ($\varepsilon$ [$10^4\times$L mol$^{-1}$ cm$^{-1}$][a] | $\lambda_{em}$ [nm] ($\tau_{em}$ [ns], $\Phi_{em}$) RT[b] | $\lambda_{em}$ [nm] ($\tau_{em}$ [μs]) 77 K[d] | $\lambda_{S1-Sn}$ [nm] ($\tau_S$ [ps])[e] | $\lambda_{T1-Tn}$ [nm] ($\tau_{TA}$ [ns], $\varepsilon_{T1-Tn}$ [$10^4\times$L mol$^{-1}$ cm$^{-1}$], $\Phi_T$)[f] |
|---|---|---|---|---|---|
| **1a** | 310 (7.70), 324 (7.82), 391 (1.31) | 577 (305, 0.023) | 525 (3.7), 561 (3.5) | 552 (103±4), 700 (110±4) | 568 (750, 4.07, 0.41) |
| **1b** | 365 (7.37), 432 (1.16) | 551 (4820, 0.163), 590 (sh) | 543 (33.0), 587 (31.1) | 485 (sh, 55±4), 621 (54±4) | 601 (1590, 6.25, 0.22) |
| **1c** | 289 (4.70), 397 (6.49) | 579 (–,[c] 0.017) | 565 (122.1), 611 (112.0) | 490 (120±6), 725 (120±6) | 530 (4810, 4.23, 0.16), 770 (5010, 7.51, 0.15) |
| **1d** | 369 (11.18), 449 (1.18) | 564 (9680, 0.083), 603 (sh) | 562 (87.0), 610 (83.7) | 600 (255±42) | 589 (1490, 8.41, 0.18) |
| **1e** | 297 (7.07), 371 (9.77), 459 (1.10) | 590 (–)[c] | 543 (8.9), 585 (7.2) | 519 (270±5) | 517 (–)[c] |

[a] Electronic absorption band maxima and molar extinction coefficients in $CH_2Cl_2$ at room temperature. [b] Room temperature emission band maxima and decay lifetimes measured in $CH_2Cl_2$ at a concentration of $1\times10^{-5}$ mol L$^{-1}$. A degassed aqueous solution of $[Ru(bpy)_3]Cl_2$ ($\Phi_{em}=0.042$, excited at 436 nm) was used as the reference. [c] Too weak to be measured. [d] The emission band maxima and decay lifetimes at 77 K measured in MTHF glassy solution at a concentration of $1\times10^{-5}$ mol L$^{-1}$. [e] Femtosecond TA band maxima and singlet excited-state lifetimes in $CH_3CN/CH_2Cl_2$ mixture (v/v): **1a**, 1:1; **1b**, 9:1; **1c**, 12:1; **1d**, 9:1; **1e**, 1:1. [f] Nanosecond TA band maxima, triplet extinction coefficients, triplet excited-state lifetimes and quantum yields in $CH_3CN/CH_2Cl_2$ mixture (9:1, v/v). SiNc in $C_6H_6$ was used as the reference. ($\varepsilon_{590}=70000$ L mol$^{-1}$ cm$^{-1}$, $\Phi_T=0.20$).

**DFT calculations**: To understand the nature of the ground and low-lying excited electronic states of **1a**–**1e**, DFT calculations were performed on these complexes in $CH_2Cl_2$. Figure 3 shows the ground-state electron density distribution

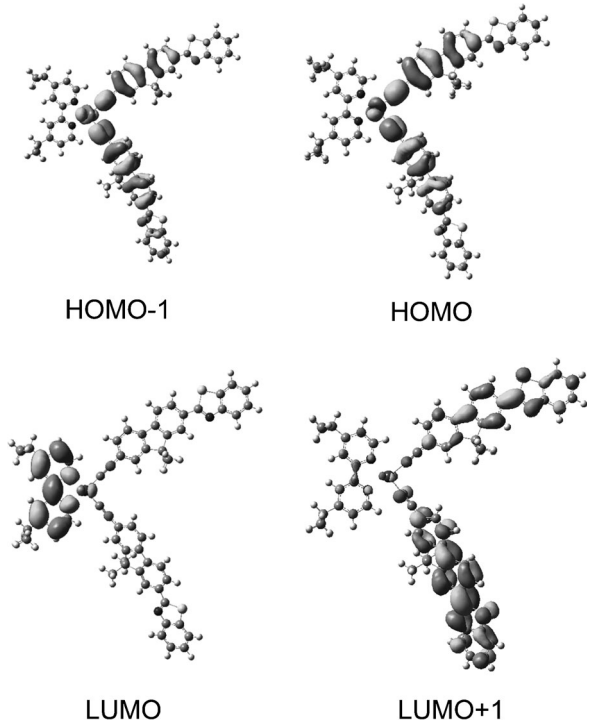


Figure 3. Contour plots of the highest occupied molecular orbital (HOMO), HOMO−1, lowest unoccupied molecular orbital (LUMO) and LUMO+1 for complex **1d**.

of the HOMO, HOMO−1, LUMO and LUMO+1 for complex **1d**, and similar data are presented in the Supporting Information for complexes **1a**, **1b**, **1c** and **1e** (Figures S10–13). The calculation results indicate that the compositions of the HOMO and HOMO−1 are quite similar for all complexes, with dominant contribution from the acetylide ligands and considerable contribution from Pt. However, different d orbitals contribute to the HOMO and HOMO−1. The LUMOs comprise almost exclusively of π*(bipyridine) in complexes **1a**, **1b**, **1d** and **1e**, whereas the electron density distribution of the LUMO for **1c** is delocalized on the bipyridine and acetylide ligands. The LUMO+1 orbitals in complexes **1a** and **1e** resemble the LUMOs, with the electron density being localized on the π*(bipyridine) moiety. However, in complexes containing electron-withdrawing substituents on the fluorenyl motifs (i.e., **1b**, **1c**, and **1d**), the dominant contributions to LUMO+1 are almost exclusively from the two acetylide ligands.

Simulations of theoretical UV/Vis absorption spectra were carried out by using the time-dependent density functional theory (TDDFT) method. Vertical excitation energies corresponding to electronic transitions from the ground state to various low-lying excited singlet electronic states were computed. The excitation energies (eV), wavelengths (nm), oscillator strengths, main contributing transitions, and the associated configuration coefficients of several low-lying electronic states of complexes **1a**–**1e** obtained at the CAM-B3LYP/LANG631//B3LYP/LANG631 level of theory are provided in Table 2 and in Supporting Information Tables S1–S4. The calculation results show that the main low-energy electronic transitions involving the HOMO→LUMO and HOMO−1→LUMO orbital pairs, which correspond to the 1st and 2nd excited states, respectively, occur at 371 and 356 nm for **1a**, 372 and 356 nm for **1b**, 378 and 364 nm for **1c**, 375 and 360 nm for **1d**, and 383 and 366 nm for **1e**. These results are in good agreement with the experimental UV/Vis absorption spectra measured in $CH_2Cl_2$. According to the electron density distribution of the HOMO−1s, HOMOs, and LUMOs, the lowest-energy absorption bands for these complexes should arise from the $^1$LLCT/$^1$MLCT transitions for **1a**, **1b**, **1d** and **1e**, and from $^1$LLCT/$^1$MLCT/$^1\pi,\pi^*$ transitions for **1c**. Transitions involving the HOMO→LUMO+1 orbital pair as dominant configurations appear at 307 nm (4th excited state) for **1a**, 332 nm (3rd excited state) for **1b**, 344 and 333 nm (3rd and 4th excited states, respectively) for **1d**, and 332 nm (3rd excited state) for **1e**, which correspond to their respective major absorption band(s) in the UV region. Therefore, DFT and TDDFT calculations provide valuable information on the electronic structures of the ground and low-lying excited electronic states, which is useful in interpreting and understanding the UV/Vis absorption spectra observed for complexes **1a**–**1e**.

Table 2. Excitation energies (eV), wavelengths (nm), oscillator strengths, main contributing transitions, and the associated configuration coefficient of five low-lying electronic states of complex **1d** obtained at the CAM-B3LYP/LANG631//B3LYP/LANG631[a] level of theory.

| $S_n$ | Excitation energy | | $f$ | Main contributing transition(s) | Configuration coefficient |
|---|---|---|---|---|---|
| | [eV] | [nm] | | | |
| 1 | 3.31 | 375 | 1.1049 | HOMO→LUMO | 0.56 |
| 2 | 3.44 | 360 | 1.4996 | HOMO−1→LUMO | 0.53 |
| 3 | 3.60 | 344 | 1.0836 | HOMO→LUMO+1 | 0.42 |
| | | | | HOMO−1→LUMO+2 | 0.34 |
| 4 | 3.72 | 333 | 0.7244 | HOMO−1→LUMO+1 | 0.39 |
| | | | | HOMO→LUMO+1 | 0.38 |
| 10 | 4.54 | 273 | 0.2765 | HOMO−14→LUMO | 0.38 |
| | | | | HOMO−15→LUMO | 0.29 |

[a] LANG631 basis set refers to 6–31G* for C, H, N and S and LANL2DZ ECP for Pt.

**Emission**: The emission characteristics of complexes **1a**–**1e** in a variety of solvents were investigated at room temperature. The concentration-dependency study was carried out in $CH_2Cl_2$ as well. The normalized emission spectra of these complexes in $CH_2Cl_2$ at a concentration of $1\times10^{-5}$ mol L$^{-1}$ are displayed in Figure 4, and the emission lifetimes and quantum yields are listed in Table 1. Excitation of these complexes in $CH_2Cl_2$ solution at their respective charge-

  

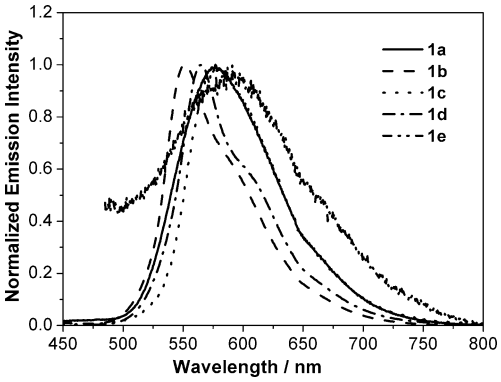


Figure 4. Normalized emission spectra of **1a**–**1e** in $CH_2Cl_2$ ($1\times10^{-5}$ mol $L^{-1}$). The excitation wavelength was 393 nm for **1a**, 376 nm for **1b**, 397 nm for **1c**, 394 nm for **1d**, and 475 nm for **1e**. Note that the emission spectra of **1a** and **1c** overlap at the longer wavelengths.

transfer band at room temperature resulted in orange to red luminescence. The emission exhibits significant Stokes shifts, and the emission lifetimes in degassed $CH_2Cl_2$ solutions vary from hundreds of nanoseconds to approximately 10 μs (except for **1c** and **1e**, which are too weak to be measured). In addition, the emission is quite sensitive to oxygen quenching. Taking all these facts into account, the observed emission from these complexes can be assigned as phosphorescence from a triplet excited state. However, the nature of the emitting state varies in different solvents. Except for **1c** and **1e**, the other complexes exhibit a negative solvatochromic effect (exemplified in Figure 5 for complex **1b** and in Supporting Information Figures S14–S16 for complexes **1a**, **1c** and **1d**). The emission energies, lifetimes and quantum yields in different solvents for **1a**–**1e** are summarized in Table 3.

As shown in Figure 5 for **1b**, in polar solvents such as $CH_3CN$ and $CH_2Cl_2$, a slight vibronic structure is observed with a vibronic spacing of approximately 1220 $cm^{-1}$, which corresponds to the ring breathing mode of the aromatic ring. Meanwhile, in polar solvents, the spectral feature and energy of the emission are influenced slightly by the polarity

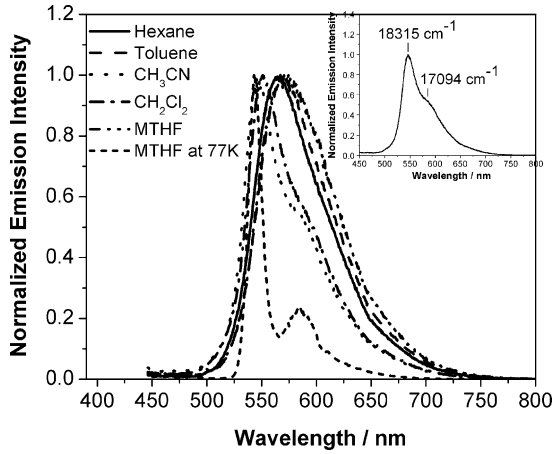


Figure 5. Normalized emission spectra of **1b** in different solvents at room temperature and in MTHF glassy matrix at 77 K. Inset: the normalized emission spectrum of **1b** in $CH_3CN$; $\lambda_{ex}=436$ nm.

Table 3. Emission energies, lifetimes and quantum yields of **1a**–**1e** in different solvents at room temperature.

| | $\lambda_{em}$ [nm] ($\tau_{em}$ [ns]; $\Phi_{em}$)[a] | | | | |
|---|---|---|---|---|---|
| | $CH_3CN$ | MTHF | $CH_2Cl_2$ | hexane | toluene |
| **1a** | 574 (120; 0.009) | 596 (200; 0.016) | 577 (310; 0.023) | 586 (320; 0.033) | 591 (290; 0.032) |
| **1b** | 546 (2070; 0.013) | 574 (680; 0.034) | 551 (4820; 0.16) | 565 (1480; 0.052) | 570 (1030; 0.045) |
| **1c** | 588 (–;[b] 0.004) | 570 (5190; 0.12) | 579 (–;[b] 0.017) | 567 (3110; 0.48) | 568 (3750; 0.37) |
| **1d** | 560 (10360; 0.044) | 586 (700; 0.152) | 564 (9680; 0.083) | 581 (970; 0.251) | 585 (740; 0.178) |
| **1e** | –[b] | –[b] | 590 (–)[b] | –[b] | –[b] |

[a] A degassed aqueous solution of $[Ru(bpy)_3]Cl_2$ ($\Phi_{em}=0.042$, excited at 436 nm) was used as the reference. [b] Too weak to be measured.

of the solvent. Therefore, the emitting state could be dominated by the $^3\pi,\pi^*$ state that is mainly localized on the acetylide ligands. The weak solvent quenching in a coordinating solvent, such as $CH_3CN$, also supports this assignment. On the contrary, in low-polarity solvents, such as hexane, MTHF (2-methyltetrahydrofuran) and toluene, the emission band is red-shifted and becomes structureless. The lifetimes also become much shorter compared to those in polar solvents. This indicates that the emitting state in low-polarity solvent is likely a charge-transfer state, that is, the $^3$MLCT state. The different solvent-dependency of the $^3\pi,\pi^*$ and $^3$MLCT states causes the switch of these two emitting states. The $^3\pi,\pi^*$ state is much less affected by the polarity of solvent, whereas the $^3$MLCT excited state becomes more stabilized in low-polarity solvent. Consequently, the energy of the $^3$MLCT excited state decreases more than the $^3\pi,\pi^*$ state and becomes the lowest excited state in low-polarity solvents, which causes the structureless and relatively short-lived emission. A similar phenomenon was observed in the emission of complex **1d** (Supporting Information Figure S16). Solvent-induced switch between the two emitting states in proximity was also found in similar platinum diimine complexes reported previously by Castellano's group[3b] and by our group.[6a]

In the emission spectra of complex **1a** (Supporting Information Figure S14), a more salient quenching in coordinating solvent was observed. The lifetimes in both polar solvent and low-polarity solvent are several hundreds of nanoseconds and the spectra become featureless in polar solvents. This suggests that the emitting state of **1a** is predominantly a $^3$MLCT state. In the case of complex **1c** (Supporting Information Figure S15), a positive solvatochromic effect was observed. The emission was significantly quenched in polar solvents, such as $CH_3CN$ and $CH_2Cl_2$. In low-polarity solvents, the emission band exhibits more structured features and is blue-shifted. The lifetime also becomes much longer compared to those in polar solvents. This is indicative of a charge-transfer emitting state. It is noted that in the solvent-dependency study of complex **1e**, only a very weak emission band was observed in $CH_2Cl_2$. Considering the strong emission of its respective ligand **2e** in different solvents (Supporting Information Figure S20), we ascribe the drastically

  

reduced emission of **1e** to the enhanced intramolecular charge-transfer state, particularly the $^3$LLCT state caused by the electron-donating $NPh_2$ group in the platinum complex.

Complexes **1a**–**1e** are also emissive in MTHF glassy matrix at 77 K (exemplified in Figure 5 for complex **1b** and in Supporting Information Figures S21–S25 for the other complexes). The emission spectra of these complexes at 77 K are blue-shifted and become narrower and more structured. The lifetimes are much longer than those at room temperature. However, the thermally induced Stokes shifts for these complexes are quite different. Complexes **1a** and **1e** exhibit relatively large thermally induced Stokes shifts, which are approximately 1720 $cm^{-1}$ for **1a** and 1470 $cm^{-1}$ for **1e**. In contrast, the thermally induced Stokes shifts for **1b**, **1c**, and **1d** are quite small (several hundreds of wavenumbers). These features, along with the vibronic structure and the long lifetime, confirm that the emission of **1b**, **1c**, and **1d** predominantly emanates from the $^3\pi,\pi^*$ excited state of the acetylide ligands at 77 K. For **1a** and **1e**, the emitting states should be ascribed to a charge-transfer excited state, likely the $^3$MLCT state. It appears that electron-withdrawing substituents, such as CHO, $NO_2$ and BTZ, significantly admix the $^3\pi,\pi^*$ character into the lowest triplet excited state, whereas electron-donating substituents retain the charge-transfer character in the lowest triplet excited state of the complex.

**Transient absorption**: Transient absorption (TA) spectroscopy provides the absorption difference between the ground state and the excited state at a given wavelength. It can predict the spectral region where reverse saturable absorption occurs. Furthermore, the lifetimes of the excited state could be obtained from the decay of the transient absorption. This is especially important for measuring the singlet excited-state lifetime of the $Pt^{II}$ complexes that cannot be obtained from the decay of fluorescence because of the very weak, undetectable fluorescence in many cases. The femtosecond (fs) and nanosecond (ns) transient absorption spectra of the complexes were studied to understand the excited-state behaviors of both singlet and triplet excited states. The time-resolved fs transient difference absorption spectra of complexes **1a**–**1e** in $CH_3CN/CH_2Cl_2$ are presented in Figure 6, and the singlet excited-state lifetimes deduced from the fs TA decay profiles are listed in Table 1.

As shown in Figure 6, complexes **1a**–**1e** all exhibit broad positive absorption band(s) from 450 to 800 nm. The shapes of the TA spectra of complexes **1a**, **1b** and **1d** are similar in that they all possess a very broad absorption band. Compared to **1a**, the TA spectra of **1b** and **1d** with electron-withdrawing substituents show significant blue-shifts, 79 and 100 nm for **1b** and **1d**, respectively, whereas complex **1e** with electron-donating substituent also exhibits a large blue-shift but with obviously different spectral feature. The fs TA spectra of the complexes are quite different from those of

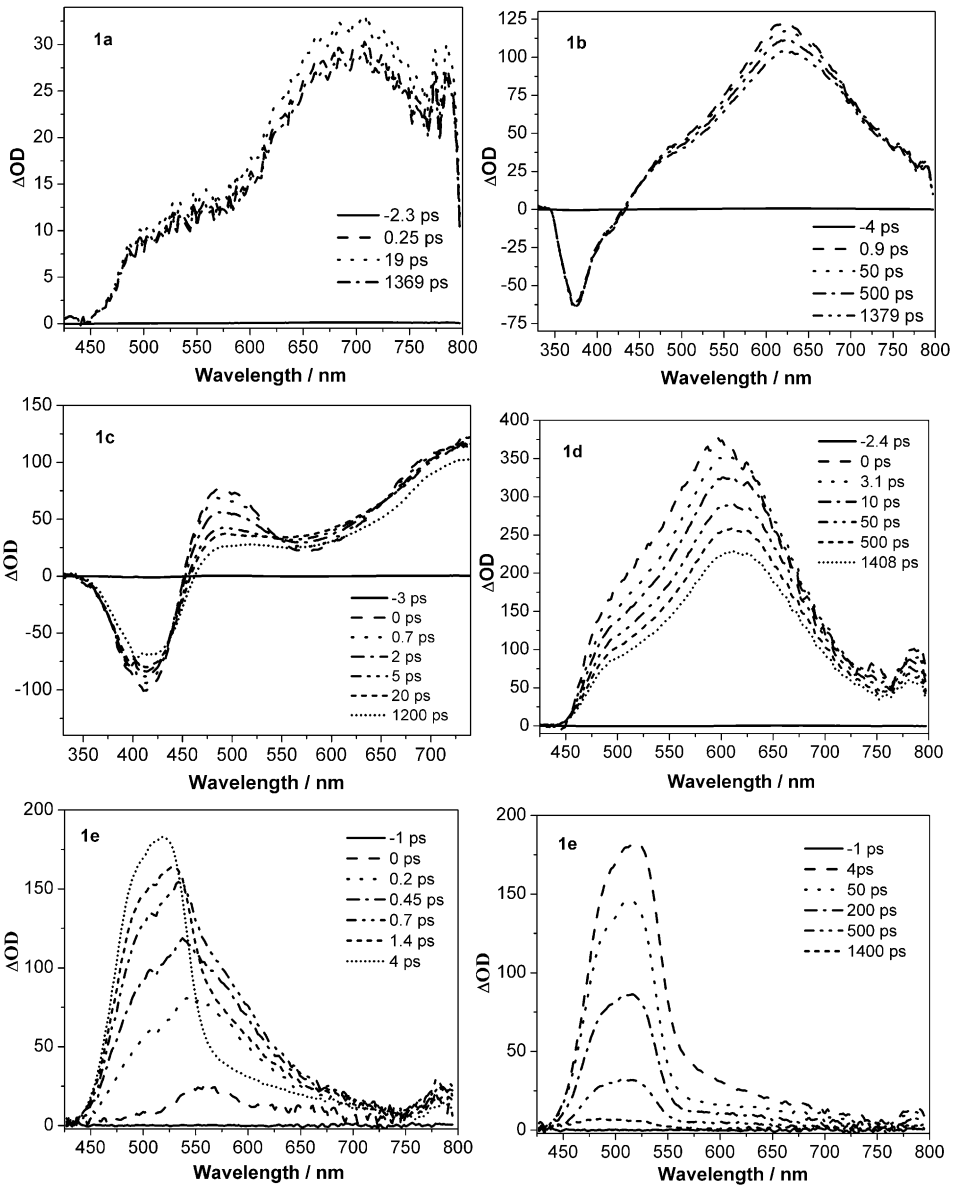


Figure 6. Time-resolved femtosecond transient difference absorption spectra of **1a**–**1e** in $CH_3CN/CH_2Cl_2$ mixture (v/v: **1a**, 1:1; **1b**, 9:1; **1c**, 12:1; **1d**, 9:1; **1e**, 1:1).

their respective ligands (Supporting Information Figures S26–S30) except for **1d**; this indicates that the excited state that gives rise to the transient absorption of **1a**, **1b**, **1c** and **1e** should not be the $^1\pi,\pi^*$ excited state of the acetylide ligands. This is supported by the kinetics of the fs TA. Immediately following the 400 nm excitation, ultrafast intersystem crossing occurs for all complexes, which is more salient for complexes **1c** and **1e**. For example, the fs TA spectrum of **1e** shows a transition from 562 to 519 nm within 4 ps. This clearly indicates the fast intersystem crossing from the $^1$MLCT state to the $^3$MLCT state, which is consistent with the heavy Pt-atom induced strong spin-orbit coupling. After the initial few picoseconds, the shapes of TA spectra remain the same over the whole time range of our approximately 1.4 ns delay line, which are essentially the same as those measured by ns laser flash photolysis (Supporting Information Figures S31–S39), except for complex **1a**. For all complexes, the shoulder at around 500 nm could be assigned to the absorption from the bipyridyl anion radical generated from $^3$MLCT or $^3$LLCT, which is consistent with similar observations in other platinum terpyridyl or iridium complexes.[8,9] The major band at the near-IR region (except for **1e**) of the TA spectrum is considered to arise from the acetylide ligand cation radical resulting from the $^3$LLCT, which was reported by the Castellano group for the triplet TA of platinum terpyridyl acetylide complexes.[10] However, similar to that reported earlier for a Pt complex analogous to **1d**, the TA feature of **1d** resembles that of its acetylide ligand. This character, along with the much longer lifetime of this complex with respect to the other complexes studied in this work, imply that the excited states that contribute to the observed fs and ns TA for **1d** should be predominantly the $^1\pi,\pi^*$ and $^3\pi,\pi^*$ states, possibly mixed with some MLCT/LLCT characters.

It is noted that the TA spectra of **1a**–**1e** are influenced significantly by the nature of the acetylide ligand. A strong electron-withdrawing substituent, such as $NO_2$, causes a better separation of the visible bipyridyl anion radical absorption band and the near-IR acetylide ligand cation radical absorption band, and a red-shift of the latter band. Electron-withdrawing aromatic substituent BTZ introduces more admixture of the $\pi,\pi^*$ character into the lowest excited states. In contrast, a strong electron-donating substituent ($NPh_2$) results in a much narrower and significantly weaker triplet excited state absorption.

**Reverse saturable absorption**: Transient difference absorption measurements indicate that complexes **1a**–**1d** exhibit stronger excited-state absorption than ground-state absorption in the visible to near-IR spectral region. For complex **1e**, the excited-state absorption in the visible spectral region is also stronger than that of the ground state. Therefore, reverse saturable absorption (RSA) is anticipated in the visible spectral region for all of these complexes. To demonstrate this, a nonlinear transmission experiment at 532 nm was carried out in a 2 mm cuvette in $CH_2Cl_2$ solution by using 4.1 ns laser pulses. The concentration of each complex solution was adjusted in order to obtain a linear transmission of 80% for easy comparison. The transmission versus incident energy curves are shown in Figure 7. With increased incident energy, the transmission of **1a**–**1e** decreases drastically. At high incident energy of approximately 187 μJ, the transmission drops from 80% to lower than 40%, which clearly manifests the RSA at 532 nm. The strength of the RSA for these complexes follows this trend: **1d** > **1e** > **1c** > **1b** ≅ **1a**. Among these, **1d** exhibits the strongest RSA, with an RSA threshold (defined as the incident energy at which the transmittance drops to 70% of the linear transmittance) of 19.5 μJ and the transmission decreases to 0.25 when the incident energy reaches approximately 178 μJ.

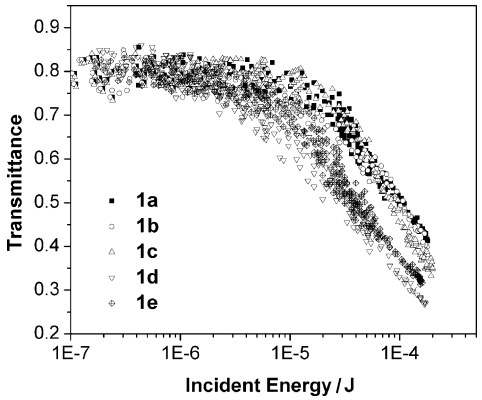


Figure 7. Nonlinear transmission curves for **1a**–**1e** in $CH_2Cl_2$ in a 2 mm cuvette for 4.1 ns laser pulses at 532 nm. The radius of the beam waist at the focal point was approximately 72 μm. The linear transmission for all samples was adjusted to 80% in a 2 mm cuvette.

Because all of the complex solutions have the same linear transmission, which guarantees the same population at the singlet excited state upon laser excitation, the observed nonlinear transmission difference should be attributed to the different ratios of the excited-state absorption cross-section to that of the ground-state ($\sigma_{ex}/\sigma_0$). The decay of the fs transient absorption discussed in the previous section indicates that these complexes possess ultrafast intersystem crossing, which completes in a few picoseconds. Therefore, the observed RSA for ns laser pulses should be dominated by the triplet excited-state absorption. In such a case, the factors that determine the strength of RSA include not only the ratio of the triplet excited-state absorption cross-section to that of the ground-state, but also the triplet excited-state quantum yields. The ground-state absorption cross-sections at 532 nm for these complexes are listed in Table 4, and are deduced from the $\varepsilon$ values obtained from their UV/Vis absorption spectra and the conversion equation $\sigma = 2303\varepsilon/N_A$, where $N_A$ is the Avogadro constant. The triplet excited-state absorption cross-sections at 532 nm are estimated from the ΔOD at zero time delay of the ns TA spectrum and the $\varepsilon_{T1-Tn}$ at the TA band maximum. The details on how to deduce the $\sigma_{ex}$ were described previously by our group for 2,4-di(2′-pyridyl)-6-(*p*-tolyl)-1,3,5-triazine platinum complexes.[12] The results are also compiled in Table 4. The $\sigma_{ex}/\sigma_0$ values for these complexes follow this trend: **1d** > **1c** > **1b** >

  

Table 4. Ground-state ($\sigma_0$) and excited-state ($\sigma_{ex}$) absorption cross-sections of the platinum complexes **1a**–**1e** at 532 nm.

| | 1a | 1b | 1c | 1d | 1e |
|---|---|---|---|---|---|
| $\sigma_0$ [$10^{-18}$ cm$^2$][a] | 0.38 | 0.36 | 0.31 | 0.39 | 0.43 |
| $\sigma_{ex}$ [$10^{-18}$ cm$^2$][b] | 79.8 | 184.3 | 167.6 | 232.6 | –[c] |
| $\sigma_{ex}/\sigma_0$ | 210.0 | 511.9 | 540.6 | 612.1 | –[c] |
| $\Phi_T\sigma_{ex}/\sigma_0$ | 86.1 | 112.6 | 86.5 | 110.2 | –[c] |

[a] In $CH_3CN$; [b] in a $CH_3CN/CH_2Cl_2$ mixture (9:1, v/v); [c] unable to detect.

**1a**. The trend implies that introducing electron-withdrawing substituent on the flourenylacetylide ligand could reduce the ground-state absorption cross-section while improving the triplet excited-state absorption cross-section, which consequently increases the ratio of the $\sigma_{ex}/\sigma_0$ and improves the RSA.

## Conclusion

A series of new platinum(II) bipyridyl complexes with different substituents on fluorenylacetylide ligands were synthesized and their photophysical properties were investigated systematically by spectroscopic techniques. The complexes exhibit ligand-centered $^1\pi,\pi^*$ transitions in the UV and blue spectral region, and broad, structureless $^1$MLCT/$^1$LLCT (for **1a**, **1b**, **1d** and **1e**) or $^1$MLCT/$^1$LLCT/$^1\pi,\pi^*$ (for **1c**) absorption bands in the visible spectral region. The assignment of the absorption bands is supported by DFT calculations. The emitting states of **1b** and **1d** exhibit a switch from the $^3\pi,\pi^*$ state in high-polarity solvents to the $^3$MLCT state in low-polarity solvents, whereas the emitting state of **1a** is predominately the $^3$MLCT state. For complexes **1c** and **1e**, the emission seems to be dominated by a triplet charge-transfer state caused by the strong electron-withdrawing or electron-donating substituent. The femtosecond transient absorption spectroscopic study indicates that these complexes exhibit ultrafast intersystem crossing. In only several picoseconds after laser excitation, the triplet excited state appears to be populated by rapid intersystem crossing. Except for complex **1e**, the triplet excited states of the other four complexes all possess broadband excited-state absorption in the visible to near-IR region. Due to the larger triplet excited-state absorption cross-section at 532 nm, strong RSA was observed at 532 nm for ns laser pulses from all of the complexes. However, the degree of RSA for these complexes at 532 nm is different, and follows the trend: **1d**>**1e**>**1c**>**1b**≅**1a**, which is a result of larger ratios of excited-state absorption cross-section to that of the ground-state in the visible to near-IR region. Consequently, complexes **1a**–**1e** could potentially be used as broadband nonlinear absorbing materials.

## Experimental Section

**Synthesis and characterization**: All solvents and reagents for synthesis were purchased from Aldrich or Alfa Aesar and were used as obtained, unless otherwise stated. Ligands **2a**,[13] **2b**,[14] **2c**,[14] **2d**,[15] and **2e**[15] were prepared according to literature procedures. All the HPLC-grade solvents used for spectroscopic studies were purchased from VWR International and were used without further purification, unless otherwise stated. Silica gels used for chromatography were purchased from Alfa Aesar Company (230–400 mesh). Ligands **2a**–**2e** and complexes **1a**–**1e** were characterized by $^1$H NMR spectroscopy and elemental analyses. $^1$H NMR spectra were obtained on a Varian Oxford-400 VNMR spectrometer or a Varian Oxford-500 VNMR spectrometer. Elemental analyses were carried out by NuMega Resonance Laboratories, Inc. (San Diego, California). HRMS data for **1a**–**1e** were not obtained due to the difficulty to ionize the complexes. The synthesis details and characterization data for **4**, **3**, **1a**–**1e** are provided in the Supporting Information.

**DFT calculations**: The ground electronic states of complexes **1a**–**1e** were simulated by DFT and their excited electronic states were calculated by using the TDDFT method to simulate their theoretical UV/Vis absorption spectra. The specific DFT methods used include Becke's exchange (B3) functional, in conjunction with Lee–Yang–Parr (LYP) correlation functional, commonly known as the B3LYP method,[16] and the Coulomb attenuating model (CAM) modified version of the B3LYP method (CAM-B3LYP) developed by Handy and co-workers.[17] The B3LYP method was used for geometry optimizations and the CAM-B3LYP method was used for calculating excited electronic state transition energies. The CAM-B3LYP method is one of the recently developed DFT functionals that takes into account the long-range correction effects often encountered in the calculation of charge-transfer molecules, such as those involved in this work. The basis sets used in all calculations includes functions from the 6–31G* set[18] used to describe all light element atoms and the LANL2DZ set[19] for the Pt atom; the particular combination is abbreviated in this work as LANG631. LANL2DZ is an effective core potential (ECP) basis set, which was used to also provide some correction for the scalar relativistic effects of the Pt atom.

Full equilibrium geometry optimizations were performed for the ground electronic states of all complexes by using a tightened self-consistent field (SCF) convergence threshold of $10^{-9}$ a.u. Methyl groups were used to replace the branched alkyl chains on the bipyridine ligand and the ethyl groups on the fluorenyl motif in complexes **1a**–**1e** to simplify the calculations due to the large size of the complexes.

Excited state calculations were performed at the fully optimized ground state molecular geometry of the complexes. In addition, bulk solvent effects were included in all calculations by using the polarizable continuum model (PCM).[20] For consistency with the experiments, dichloromethane ($CH_2Cl_2$), which was used as the solvent for experimental measurements, was selected as the solvent in theoretical calculations as well. All calculations were performed by using the Gaussian 09 (Revision A.1) software suite[21] running on a 96-node distributed-memory cluster with 192 Dual 3.06 GHz Xeon-HT processors at North Dakota State University.

**Photophysical measurements**: The UV/Vis absorption spectra of **2a**–**2e** and **1a**–**1e** were obtained by using a Shimadzu UV-2501 spectrophotometer in different solvents (HPLC grade). The steady-state emission spectra were measured on a SPEX Fluorolog-3 fluorometer/phosphorometer. The emission quantum yields were measured by the relative actinometry method[22] in degassed solutions. A degassed aqueous solution of [Ru(bpy)$_3$]Cl$_2$ ($\Phi_{em}=0.042$, $\lambda_{ex}=436$ nm)[23] was used as the reference for complexes **1a**–**1e** and an aqueous solution of quinine sulfate ($\Phi_{em}=0.546$, $\lambda_{ex}=365$ nm)[24] was used as the reference for ligands **2a**–**2e**. The femtosecond transient difference absorption spectra and the singlet excited-state lifetimes were measured by using a femtosecond pump-probe UV/Vis spectrometer. The laser system for the ultrafast transient absorption measurement was described previously.[25] The laser system (Hurricane, Spectra Physics) output consisted a Ti:sapphire oscillator/regenerative amplifier as a source of 800 nm light with fwhm of 110 fs operating at a repetition rate of 1 kHz. The 800 nm light was split into pump (85%) and probe (10%) beams. A white light continuum probe beam was produced by using a $CaF_2$ crystal. The sample solution in a 2 mm flow cell was excited by using 400 nm light (~2 μJ per pulse) produced by a second harmonic generator (Super Tripler, CSK). The nanosecond transient difference absorption spectra, triplet excited-state lifetimes and trip-

  

let excited-state quantum yields were measured on an Edinburgh LP920 laser flash photolysis spectrometer. The excitation source was the third harmonic output (355 nm) of a Nd:YAG laser (Quantel Brilliant, pulsewidth ~4.1 ns, 1 Hz). Before each measurement, all the sample solutions were degassed with Ar for 30 min.

Singlet depletion method[26] was used to determine the triplet excited-state molar extinction coefficients ($\varepsilon_T$) at the TA band maximum, in which $\varepsilon_T$ was calculated by the following equation:[26]

$$\varepsilon_T = \varepsilon_S \frac{\Delta OD_T}{\Delta OD_S} \quad (1)$$

where $\varepsilon_S$ is the ground-state molar extinction coefficient at the wavelength of the bleaching band minimum in the TA spectrum; $\Delta OD_S$ and $\Delta OD_T$ are the optical density changes at the minimum of the bleaching band and the maximum of the positive band, respectively. When the $\varepsilon_T$ value is obtained, the triplet excited-state quantum yield can be calculated by the relative actinometry,[27] in which SiNc in benzene was used as the reference ($\varepsilon_{590}=70000\,M^{-1}cm^{-1}$, $\Phi_T=0.20$).[28]

**Nonlinear transmission measurement**: The nonlinear transmission experiments for complexes **1a–1e** at 532 nm were carried out in $CH_2Cl_2$ solution in a 2 mm cuvette by using 4.1 ns laser pulses. A Quantel Brilliant ns laser with a repetition rate of 10 Hz was used as the light source. The experimental setup and details were described previously.[29] An $f=30$ cm plano-convex lens was used to focus the beam to the sample cuvette. The radius of the beam waist at the focal point is approximately 72 μm measured by knife edge. The linear transmission of the solution was adjusted to 80% in the 2 mm cuvette.

**Supporting information**: Synthesis details and characterization data, UV/Vis absorption spectra of **2a–2e** in $CH_2Cl_2$. Normalized UV/Vis absorption and emission spectra of **1a–1e** and **2a–2e** in different solvents. Normalized emission spectra of complexes **1a–1e** in MTHF at room temperature and 77 K. Contour plots and tables of the HOMO, HOMO−1, LUMO and LUMO+1 for complexes **1a**, **1b**, **1c** and **1e**. The singlet and triplet transient difference absorption spectra of **1a–1e** and **2a–2e** in $CH_3CN/CH_2Cl_2$ or in toluene.

## Acknowledgements

This work is partially supported by the National Science Foundation (CAREER CHE-0449598) and partially supported by the Army Research Laboratory (W911NF-06–2–0032).

[1] a) M. Hissler, J. E. McGarrah, W. B. Connick, D. K. Geiger, S. D. Cummings, R. Eisenberg, *Coord. Chem. Rev.* **2000**, *208*, 115–137; b) J. E. McGarrah, Y. J. Kim, M. Hissler, R. Eisenberg, *Inorg. Chem.* **2001**, *40*, 4510–4511; c) S. Suzuki, R. Sugimura, M. Kozaki, K. Keyaki, K. Nozaki, N. Ikeda, K. Akiyama, K. Okada, *J. Am. Chem. Soc.* **2009**, *131*, 10374–10375.

[2] a) H. Guo, S. Ji, W. Wu, W. Wu, J. Shao, J. Zhao, *Analyst* **2010**, *135*, 2832–2840; b) H. Guo, M. L. Muro-Small, S. Ji, J. Zhao, F. N. Castellano, *Inorg. Chem.* **2010**, *49*, 6802–6804.

[3] a) S. C. Chan, M. C. W. Chan, Y. Wang, C. M. Che, K. K. Cheung, N. Zhu, *Chem. Eur. J.* **2001**, *7*, 4180–4190; b) I. E. Pomestchenko, F. N. Castellano, *J. Phys. Chem. A* **2004**, *108*, 3485–3492; c) I. E. Pomestchenko, C. R. Luman, M. Hissler, R. Ziessel, F. N. Castellano, *Inorg. Chem.* **2003**, *42*, 1394–1396.

[4] a) T. J. Wadas, R. J. Lachicotte, R. Eisenberg, *Inorg. Chem.* **2003**, *42*, 3772–3778; b) M. Hissler, W. B. Connick, D. K. Geiger, J. E. McGarrah, D. Lipa, R. J. Lachicotte, R. Eisenberg, *Inorg. Chem.* **2000**, *39*, 447–457; c) C. E. Whittle, J. A. Weinstein, M. W. George, K. S. Schanze, *Inorg. Chem.* **2001**, *40*, 4053–4062.

[5] K. Haskins-Glusac, I. Ghiviriga, K. A. Abboud, K. S. Schanze, *J. Phys. Chem. B* **2004**, *108*, 4969–4978.

[6] a) W. Sun, B. Zhang, Y. Li, T. M. Pritchett, Z. Li, J. E. Haley, *Chem. Mater.* **2010**, *22*, 6384–6392; b) T. M. Pritchett, W. Sun, B. Zhang, M. J. Ferry, Y. Li, J. E. Haley, D. M. Mackie, W. Shensky III, A. G. Mott, *Opt. Lett.* **2010**, *35*, 1305–1307.

[7] Z. Li, E. Badaeva, D. Zhou, J. Bjorgaard, K. D. Glusac, S. Killina, W. Sun, *J. Phys. Chem. A* **2012**, *116*, 4878–4889.

[8] E. Shikhova, E. O. Danilov, S. Kinayyigit, I. E. Pomestchenko, A. D. Tregubov, F. Camerel, P. Retailleau, R. Ziessel, F. N. Castellano, *Inorg. Chem.* **2007**, *46*, 3038–3048.

[9] F. Spaenig, J.-H. Oliver, V. Prusakova, P. Retailleau, R. Ziessel, F. N. Castellano, *Inorg. Chem.* **2011**, *50*, 10859–10871.

[10] X. Wang, S. Geob, Z. Ji, F. N. Castellano, *J. Phys. Chem. B* **2010**, *114*, 14440–14449.

[11] a) J. Vicente, P. Gonzalez-Herrero, M. Perez-Cadenas, P. G. Jones, D. Bautista, *Inorg. Chem.* **2007**, *46*, 4718–4732; b) L. M. Rendina, J. J. Vittal, R. J. Puddephatt, *Organometallics* **1995**, *14*, 1030–1038; c) C. J. Adams, S. L. James, X. Liu, P. R. Raithby, L. J. Yellowlees, *J. Chem. Soc. Dalton Trans.* **2000**, 63–67.

[12] P. Shao, Y. Li, W. Sun, *Organometallics* **2008**, *27*, 2743–2749.

[13] L. Liu, W. Y. Wong, Y. W. Lam, W. Y. Tam, *Inorg. Chim. Acta* **2007**, *360*, 109–121.

[14] J. E. Haley, D. M. Krein, J. L. Monahan, A. R. Burke, D. G. McLean, J. E. Slagle, A. Fratini, T. M. Cooper, *J. Phys. Chem. A* **2011**, *115*, 265–273.

[15] J. E. Rogers, J. E. Slagle, D. M. Krein, A. R. Burke, B. C. Hall, A. Fratini, D. G. McLean, P. A. Fleitz, T. M. Cooper, M. Drobizhev, N. S. Makarov, A. Rebane, K. Y. Kim, R. Farley, K. S. Schanze, *Inorg. Chem.* **2007**, *46*, 6483–6494.

[16] a) A. D. Becke, *J. Chem. Phys.* **1993**, *98*, 5648–5652; b) C. Lee, W. Yang, R. G. Parr, *Phys. Rev. B* **1988**, *37*, 785–789.

[17] T. Yanai, D. P. Tew, N. C. Handy, *Chem. Phys. Lett.* **2004**, *393*, 51–57.

[18] a) T. Clark, J. Chandrasekhar, G. W. Spitznagel, P. V. R. Schleyer, *J. Comput. Chem.* **1983**, *4*, 294–301; b) M. M. Francl, W. J. Pietro, W. J. Hehre, J. S. Binkley, M. S. Gordon, D. J. DeFrees, J. A. Pople, *J. Chem. Phys.* **1982**, *77*, 3654–3665; c) P. M. W. Gill, B. G. Johnson, J. A. Pople, M. J. Frisch, *Chem. Phys. Lett.* **1992**, *197*, 499–505; d) P. C. Hariharan, J. A. Pople, *Theor. Chim. Acta* **1973**, *28*, 213–222; e) R. Krishnan, J. S. Binkley, R. Seeger, J. A. Pople, *J. Chem. Phys.* **1980**, *72*, 650–654.

[19] a) P. J. Hay, W. R. Wadt, *J. Chem. Phys.* **1985**, *82*, 299–310; b) P. J. Hay, W. R. Wadt, *J. Chem. Phys.* **1985**, *82*, 270–283; c) W. R. Wadt, P. J. Hay, *J. Chem. Phys.* **1985**, *82*, 284–298.

[20] J. Tomasi, B. Mennucci, R. Cammi, *Chem. Rev.* **2005**, *105*, 2999–3094.

[21] Gaussian 09, Revision A.1, M. J. Frisch, G. W. Trucks, H. B. Schlegel, G. E. Scuseria, M. A. Robb, J. R. Cheeseman, G. Scalmani, V. Barone, B. Mennucci, G. A. Petersson, H. Nakatsuji, M. Caricato, X. Li, H. P. Hratchian, A. F. Izmaylov, J. Bloino, G. Zheng, J. L. Sonnenberg, M. Hada, M. Ehara, K. Toyota, R. Fukuda, J. Hasegawa, M. Ishida, T. Nakajima et al., Gaussian, Inc., Wallingford CT, **2009**.

[22] G. A. Crosby, J. N. Demas, *J. Phys. Chem.* **1971**, *75*, 991–1024.

[23] J. Van Houten, R. J. Watts, *J. Am. Chem. Soc.* **1976**, *98*, 4853–4858.

[24] W. H. Melhuish, *J. Phys. Chem.* **1961**, *65*, 229–235.

[25] D. Zhou, E. Mirzakulova, R. Khatmullin, I. Schapiro, M. Olivucci, K. D. Glusac, *J. Phys. Chem. B* **2011**, *115*, 7136–7143.

[26] I. Carmichael, G. L. J. Hug, *J. Phys. Chem. Ref. Data* **1986**, *15*, 1–250.

[27] C. V. Kumar, L. Qin, P. K. Das, *J. Chem. Soc. Faraday Trans. 2* **1984**, *80*, 783–793.

[28] P. A. Firey, W. E. Ford, J. R. Sounik, M. E. Kenney, M. A. J. Rodgers, *J. Am. Chem. Soc.* **1988**, *110*, 7626–7630.

[29] W. Sun, H. Zhu, P. M. Barron, *Chem. Mater.* **2006**, *18*, 2602–2610.

Received: January 23, 2012
Revised: May 18, 2012
Published online: July 30, 2012

  